ARTICLE NO. 80-4088

J80-202

20015
20017

Analytical Solution of Double-Mach Reflection

G. Ben-Dor*
Ben-Gurion University of the Negev, Beer-Sheva, Israel

The double-Mach reflection (DMR) of oblique shock waves in pseudo-stationary flows has been investigated. The equations of motion of the first and second triple point were formulated, as well as the relative motion between these two triple points. The equation of motion for each triple point consists of 14 nonlinear algebraic equations. An analytical method of solution is presented. Consequently, for the first time a complete analytical solution of a DMR is given. Utilizing this analytical solution a method for predicting the second triple-point trajectory angle is developed. The analytical results are compared with experiments that were performed on the 10×18 cm Hypervelocity Shock Tube at the University of Toronto Institute for Aeronautical Studies. Good agreement was obtained.

Introduction

WHEN a planar moving-incident shock wave encounters a sharp compressive corner in a shock tube, four different shock-wave reflections can occur, depending upon the Mach number of the incident shock wave M_s, the corner wedge angle θ_w, and the initial thermodynamic state of the gas (i.e., temperature T_0 and pressure P_0), although for a perfect gas this is not required. The four different shock-wave reflections are shown in Fig. 1: a) regular reflection (RR), b) single-Mach reflection (SMR), c) complex-Mach reflection (CMR), and d) double-Mach reflection (DMR).

Although these four reflections were all observed by 1951, their domains and transitions in both diatomic[1] and monatomic[2] gases have been established analytically and experimentally only recently. This was done by solving the 14 nonlinear oblique-shock-wave equations that describe the triple point of SMR, CMR, and DMR analytically for both perfect and imperfect monatomic and diatomic gases. This unique method of solution is presented subsequently.

Figure 2 represents the domains and transition boundaries of nonstationary oblique-shock-wave diffractions in the (M_s,θ_w) plane for imperfect nitrogen ($P_0=15$ Torr, $T_0=300$K). It is seen that in the range $1<M_s<10$ two different diffractions of DMR are possible. In one of them the shock wave at the wedge corner is detached (region 6), while in the other it is attached (region 7). Further details concerning this figure can be found in Refs. 1 and 3.

Unlike RR and SMR, which are understood and well covered analytically and experimentally in the literature,[1-25] CMR and DMR have been treated mainly experimentally [Refs. 5 and 9 (discovery of CMR and DMR, respectively), 13-15, and 18]. Since in all of these works the main emphasis was on deducing quantitative results from experiments, CMR and DMR were somewhat ignored analytically. Consequently, it was decided to undertake a detailed study of the DMR in an effort to bring more light and understanding into this complicated reflection. We believe the major reason that CMR and DMR have not been as well treated as RR and SMR is probably due to the difficulty arising from the fact that in order to treat them correctly, one has to attach the frame of reference to the kink K of a CMR or the second triple point T_1 of a DMR. Consequently, the correct transformation from the first triple point T to the second triple point T_1 should be understood and formulated. To the best of our knowledge this transformation has never been reported. During the course of the present research we were able to formulate this transformation correctly. As a consequence, an analytical method for the prediction of the second triple-point trajectory angle χ' was developed. This method complements the analytical method reported by Ben-Dor and Glass[1,2] for the prediction of the first triple-point trajectory angle χ. The analytical predictions were substantiated by experimental results which were obtained in the 10×18 cm UTIAS Hypervelocity Shock Tube.

Analysis

It has been shown by Ben-Dor and Glass[1] that, in order for a DMR to form, the flow in region 2 behind the reflected shock wave R should become supersonic with respect to the kink K of a CMR (Figs. 1c and 1d). Consequently, if M_{ij} is the Mach number of the flow in region (i) with respect to (j), the CMR ⇌ DMR transition criterion is:

$$M_{2K}=1 \tag{1}$$

It is worthwhile mentioning that it was further found that the transition boundary line arising from this criterion can also be

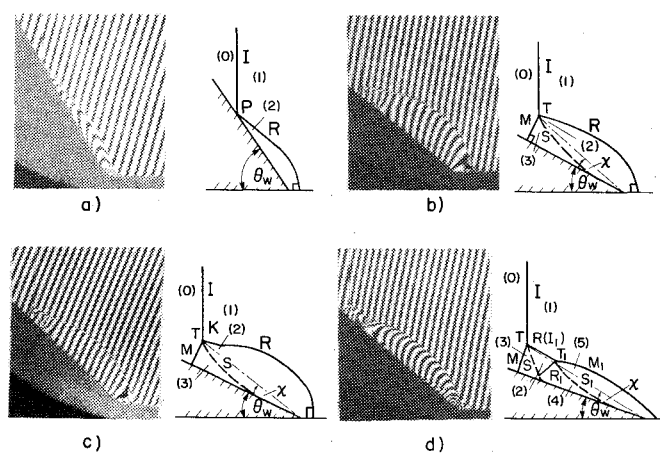

Fig. 1 Four possible oblique-shock-wave reflections. Interferograms (λ = 6943 Å) were taken with 23-cm-diam field of view Mach-Zehnder Interferometer in the UTIAS 10×18 cm Hypervelocity Shock Tube for nitrogen at initial pressure $P_0\approx 15$ Torr and temperature $T_0\approx 300$ K. I, I_1 = incident shock waves; R, R_1 = reflected shock waves; M, M_1 = Mach stems; S, S_1 = slipstreams; T, T_1 = triple points; K = kink; χ, χ' = triple point trajectory angles; 0-5 = thermodynamic states. a) Regular reflection (RR), wedge angle $\theta_w=60$ deg, shock Mach number $M_s=4.68$; b) single-Mach reflection (SMR), $\theta_w=10$ deg, $M_s=4.72$; c) complex-Mach reflection (CMR), $\theta_w=20$ deg, $M_s=6.90$; d) double-Mach reflection (DMR), $\theta_w=40$ deg, $M_s=3.76$.

Received April 19, 1979; revision received Sept. 21, 1979.

Index categories: Shock Waves and Detonations; Supersonic and Hypersonic Flows.

*Department of Mechanical Engineering. Member AIAA.

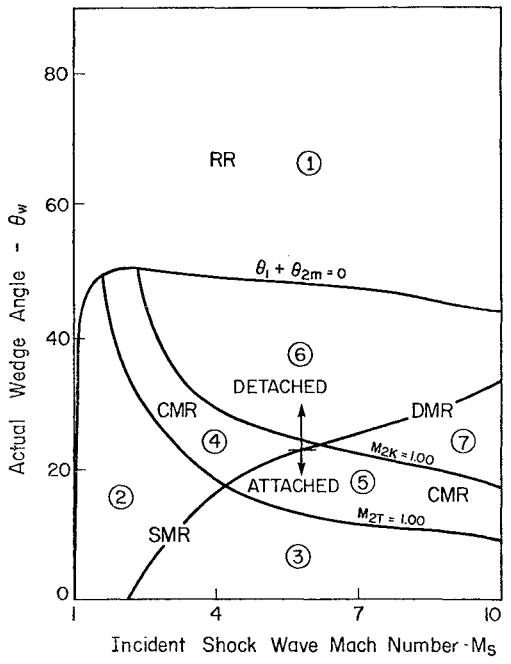

Fig. 2 Domains of different oblique-shock-wave diffractions in (M_s,θ_w) plane (lines are for imperfect nitrogen with $P_0 = 15$ Torr and $T_0 = 300$ K): 1) RR with detached shock wave at wedge corner (detached RR), 2) detached SMR, 3) attached SMR, 4) detached CMR, 5) attached CMR, 6) detached DMR, 7) attached DMR.

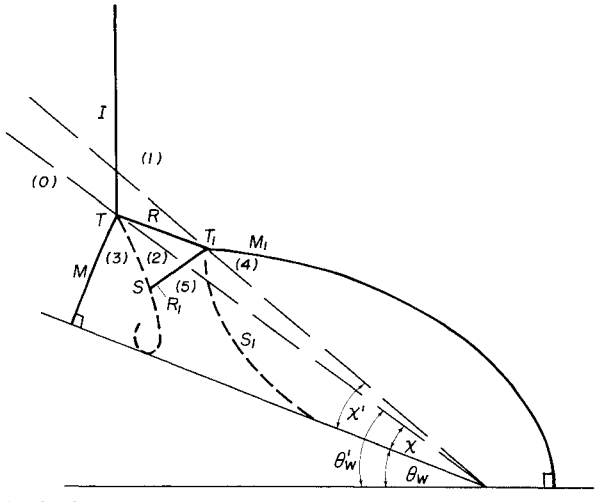

Fig. 3 Schematic diagram of DMR configuration: I, I_1, R, R_1, M, M_1, S, S_1, T, T_1, χ, χ', θ_w, states 0-5 as defined in Fig. 1; $\theta'_w = \theta_w + \chi$.

described quite well by:

$$M_{2T} \approx 1.30 \tag{1a}$$

A detailed shock-wave configuration of a DMR is shown in Fig. 3. Two three-shock confluences (triple points) T and T_1 are clearly seen. Each consist of three shock waves (I,R,M, and R,R_1,M_1, respectively) and one slipstream (S and S_1). The first shock wave is usually termed incident, the second reflected, and the third Mach stem. Note that while R is the reflected shock wave of the first triple point T, it is the incident shock wave of the second three-shock confluence T_1. Each slipstream separates two different thermodynamic states with equal pressure and flow direction. The shock-wave configuration is self-similar[8,26] and since it started to grow from the moment the incident shock wave I collided with the compression corner, the triple points T and T_1 should move in the laboratory coordinates along straight lines emanating from the corner. These two lines form the corresponding triple-point trajectory angles χ and χ' with the wedge surface.

Analytical Formulation

In a frame of reference attached to the first triple point, the incident and reflected shock waves (I and R) and the Mach stem (M) can be treated using steady-flow theory. Using the well-known oblique-shock-wave relations across I, R, and M one obtains for I:

$$\rho_0 \tan\phi_1 = \rho_1 \tan(\phi_1 - \theta_1) \tag{2}$$

$$\rho_0 U_0 \sin\phi_1 = \rho_1 U_1 \sin(\phi_1 - \theta_1) \tag{3}$$

$$P_0 + \rho_0 U_0^2 \sin^2\phi_1 = P_1 + \rho_1 U_1^2 \sin^2(\phi_1 - \theta_1) \tag{4}$$

$$h_0 + \tfrac{1}{2} U_0^2 \sin^2\phi_1 = h_1 + \tfrac{1}{2} U_1^2 \sin^2(\phi_1 - \theta_1) \tag{5}$$

for R:

$$\rho_1 \tan\phi_2 = \rho_2 \tan(\phi_2 - \theta_2) \tag{6}$$

$$\rho_1 U_1 \sin\phi_2 = \rho_2 U_2 \sin(\phi_2 - \theta_2) \tag{7}$$

$$P_1 + \rho_1 U_1^2 \sin^2\phi_2 = P_2 + \rho_2 U_2^2 \sin^2(\phi_2 - \theta_2) \tag{8}$$

$$h_1 + \tfrac{1}{2} U_1^2 \sin^2\phi_2 = h_2 + \tfrac{1}{2} U_2^2 \sin^2(\phi_2 - \theta_2) \tag{9}$$

for M:

$$\rho_0 \tan\phi_3 = \rho_3 \tan(\phi_3 - \theta_3) \tag{10}$$

$$\rho_0 U_0 \sin\phi_3 = \rho_3 U_3 \sin(\phi_3 - \theta_3) \tag{11}$$

$$P_0 + \rho_0 U_0^2 \sin^2\phi_3 = P_3 + \rho_3 U_3^2 \sin^2(\phi_3 - \theta_3) \tag{12}$$

$$h_0 + \tfrac{1}{2} U_0^2 \sin^2\phi_3 = h_3 + \tfrac{1}{2} U_3^2 \sin^2(\phi_3 - \theta_3) \tag{13}$$

and the boundary conditions across the slipstream S imply:

$$P_2 = P_3 \tag{14}$$

$$\theta_3 = \theta_1 \mp \theta_2 \tag{15}$$

where ρ_i, P_i, h_i, and U_i are the density, pressure, enthalpy, and absolute flow velocity in state (i) and ϕ_i is the angle of incidence between the flow and the shock wave through which the flow is deflected by an angle of θ_i to become state (i).

It has been shown by Henderson[11] and Ben-Dor and Glass[1] that two different families of triple-point solutions are possible. The usual one, in which I and R deflect the flow passing through them in opposite directions so that $\theta_3 = \theta_1 - \theta_2$, and one in which the flow deflections through I and R are in the same direction, i.e., $\theta_3 = \theta_1 + \theta_2$. For the former family the minus sign is used in Eq. (15), and the plus sign applies for the latter. The correct criteria for differing between these two families a priori were calculated by Ben-Dor[3] for both perfect and imperfect, monatomic and diatomic gases.

The above 14 equations [Eqs. (2-15)] consist of 22 independent variables ($\rho_1,\rho_2,\rho_3,\rho_4,P_1,P_2,P_3,P_4,h_1,h_2,h_3,h_4$, $U_1,U_2,U_3,U_4,\phi_1,\phi_2,\phi_3,\theta_1,\theta_2$, and θ_3). Consequently, in general, 8 of these 22 parameters should be known in order to solve the remaining 14. However, if thermodynamic equilibrium is assumed, ρ_i, P_i, and h_i are no longer independent, since under these circumstances two thermodynamic properties are sufficient to define a state. As a consequence, 4 out of the above 12 thermodynamic variables vanish and one is left with 18 unknowns. Since there are 14 equations, only 4 parameters should be defined in order to

calculate the remaining 14. The four chosen parameters are the flow pressure P_0 and temperature T_0 ahead of the incident shock wave, the flow velocity $U_0[U_0 = U_s \sec(\theta_w + \chi)$ where U_s is the velocity of the incident shock wave], and the angle of incidence ϕ_1 between the flow in region 0 and the incident shock wave I [$\phi_1 = 90 - (\theta_w + \chi)$]. It is worth mentioning that upon assuming a calorically and thermally perfect gas, Henderson[11] was able to reduce the above set of equations to a single polynomial of degree 10. The polynomial coefficients were taken to be functions of γ, M_0, and P_1/P_0. (For further details, see Ref. 11.)

When real gas effects are considered, Eqs. (2-15) cannot be simplified and the 14 nonlinear equations must be solved. A unique method of solution recently developed by the present author is described as follows. It makes use of the fact that Eqs. (2-15) consist of three identical sets of equations (2-5, 6-9, and 10-13). The first set [Eqs. (2-5)] involve eight variables: P_0, T_0, U_0, and ϕ_1 on the left-hand side (LHS) and P_1, T_1, U_1, and θ_1 on the right-hand side (RHS). Note that P and T are selected as the two independent thermodynamic properties that are required to define a state, i.e., $\rho = \rho\ (P,T)$ and $h = h(P,T)$. Since the variables in the LHS are all known, the RHS can be solved to obtain P_1, T_1, U_1, and θ_1. The second set [Eqs. 6-9)] consists again of eight variables: P_1, T_1, U_1, and ϕ_2 on the LHS and P_2, T_2, U_2, and θ_2 on the RHS. Unlike the first set where all of the LHS parameters were known, here only P_1, T_1, and U_1 (obtained from the solution of the first set) are known. However, if one guesses the value of ϕ_2, this set becomes identical to the first set and can be solved in the same way to obtain P_2, T_2, U_2, and θ_2. The third set consists again of eight variables; P_0, T_0, U_0, and ϕ_3 on the LHS and P_3, T_3, U_3, and θ_3 on the RHS. Like the second set only three out of the four LHS parameters are known (P_0, T_0, and U_0). Upon guessing the value of ϕ_3 this set also becomes identical to the first set and is solved in the same fashion to give P_3, T_3, U_3, and θ_3. In the foregoing solution procedure two values have been guessed, ϕ_2 and ϕ_3. The correct values of ϕ_2 and ϕ_3 are those which will result in values of $P_2, P_3, \theta_1, \theta_2$, and θ_3 that will satisfy the boundary conditions [Eqs. (14) and (15)]. For further details and computer programs concerning the solution of Eqs. (2-15), see Ref. 3.

The analytical formulation of the second triple point is based upon the above mentioned similarity of the flowfields associated with the first and second triple points and upon an empirical approximation for the relative motion of the second triple point. Consider Figs. 4a and 4b which describe the flowfields in the vicinity of T and T_1, respectively. Let the notation $b = a$ mean that symbol b in Fig. 4b is equivalent (analogous) to symbol a in Fig. 4a. Following this notation one can write; state (1) = state (0), state (2) = state (1), state (5) = state (2), state (4) = state (3);

$$R = I,\ R_1 = R,\ M_1 = M,\ S_1 = S;$$

$$U_1' = U_0,\ U_2' = U_1,\ U_5' = U_2,\ U_4' = U_3;$$

$$\theta_2' = \theta_1,\ \theta_5' = \theta_2,\ \theta_4' = \theta_3;$$

and finally,

$$\phi_2' = \phi_1,\ \phi_5' = \phi_2,\ \text{and}\ \phi_4' = \phi_3$$

Applying this analogy to Eqs. (2-15) results in the oblique-shock-wave equations that describe the second triple point, i.e.,

for R:

$$\rho_1 \tan\phi_2' = \rho_2 \tan(\phi_2' - \theta_2') \tag{16}$$

$$\rho_1 U_1' \sin\phi_2' = \rho_2 U_2' \sin(\phi_2' - \theta_2') \tag{17}$$

$$P_1 + \rho_1 U_1'^2 \sin^2\phi_2' = P_2 + \rho_2 U_2'^2 \sin^2(\phi_2' - \theta_2') \tag{18}$$

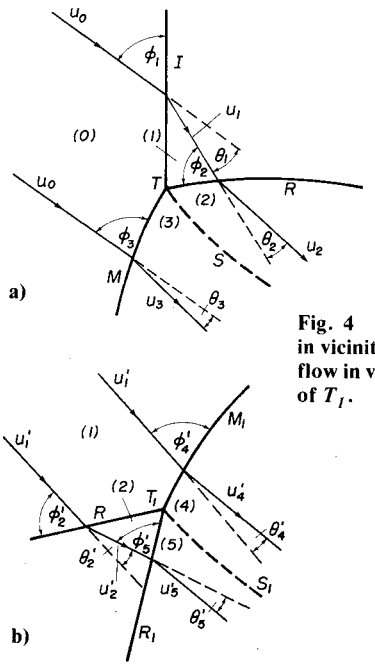

Fig. 4 Similarity between flowfields in vicinity of triple points T and T_1: a) flow in vicinity of T, b) flow in vicinity of T_1.

$$h_1 + \tfrac{1}{2} U_1'^2 \sin^2\phi_2' = h_2 + \tfrac{1}{2} U_2'^2 \sin^2(\phi_2' - \theta_2') \tag{19}$$

for R_1:

$$\rho_2 \tan\phi_5' = \rho_5 \tan(\phi_5' - \theta_5') \tag{20}$$

$$\rho_2 U_2' \sin\phi_5' = \rho_5 U_5' \sin(\phi_5' - \theta_5') \tag{21}$$

$$P_2 + \rho_2 U_2'^2 \sin^2\phi_5' = P_5 + \rho_5 U_5'^2 \sin^2(\phi_5' - \theta_5') \tag{22}$$

$$h_2 + \tfrac{1}{2} U_2'^2 \sin^2\phi_5' = h_5 + \tfrac{1}{2} U_5'^2 \sin^2(\phi_5' - \theta_5') \tag{23}$$

for M_1:

$$\rho_1 \tan\phi_4' = \rho_4 \tan(\phi_4' - \theta_4') \tag{24}$$

$$\rho_1 U_1' \sin\phi_4' = \rho_4 U_4' \sin(\phi_4' - \theta_4') \tag{25}$$

$$P_1 + \rho_1 U_1'^2 \sin^2\phi_4' = P_4 + \rho_4 U_4'^2 \sin^2(\phi_4' - \theta_4') \tag{26}$$

$$h_1 + \tfrac{1}{2} U_1'^2 \sin^2\phi_4' = h_4 + \tfrac{1}{2} U_4'^2 \sin^2(\phi_4' - \theta_4') \tag{27}$$

And finally the boundary conditions across S_1 are:

$$P_5 = P_4 \tag{28}$$

$$\theta_4' = \theta_2' \mp \theta_5' \tag{29}$$

The prime denotes that the properties are measured with respect to the second triple point. It is omitted from the thermodynamic properties since they do not depend upon the frame of reference from which they are calculated.

Since Eqs. (16-29) are identical in their form to Eqs. (2-15), they can be solved using the same procedure. To do so, the LHS parameters of the first set [Eqs. (16-19)] should be known. The thermodynamic parameters P_1 and T_1 are known from the solution of Eqs. (2-15). Therefore, only U_1' and ϕ_2' need to be calculated. Their calculation involves a transformation of the already calculated values of U_1 and ϕ_2 from a frame of reference attached to T to a frame of reference attached to T_1.

The self-similarity of the reflection phenomenon[26] (i.e., the fact that any point on the wave configuration having a radius vector $\bar{r}$ with the corner as origin is transformed to a new point $c\bar{r}$ where c is a scalar constant) implies that the angles

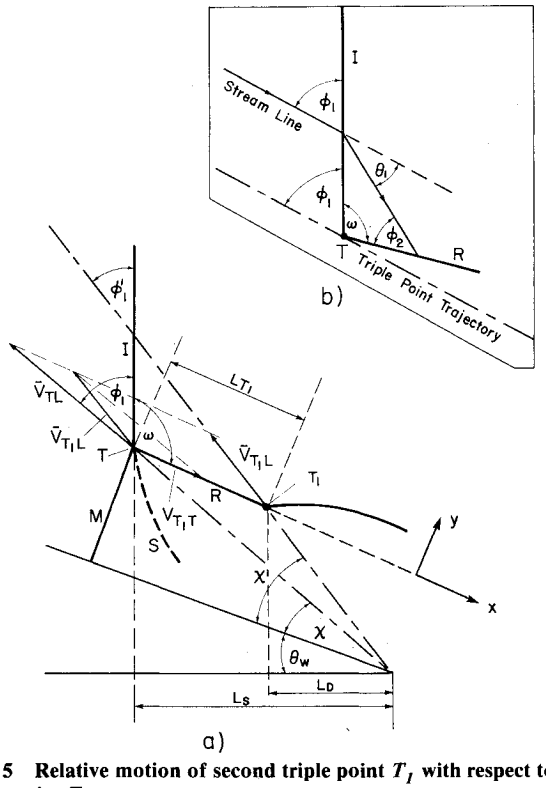

Fig. 5 Relative motion of second triple point T_1 with respect to first triple point T.

between the shock waves do not change. Consequently, the second triple point T_1 moves along a line formed by the reflected shock wave R with respect to the first triple point T.

Consider Fig. 5a in which T moves with the velocity $\bar{V}_{TL}$, in the laboratory frame of reference, along a line inclined at an angle χ to the wedge. The second triple point T_1 moves along the the line defined by R with the velocity $\bar{V}_{T_1T}$ with respect to T. In the laboratory frame of reference T_1 moves along a line inclined at an angle χ' to the wedge surface with velocity $\bar{V}_{T_1L}$. Simple vector analysis yields:

$$|\bar{V}_{TL}| = U_s \operatorname{cosec} \phi_1 \tag{30}$$

(Note $|\bar{V}_{TL}| = U_0$ by definition.) If the distance traveled by I from the moment it collided with the wedge corner is L_s, then the time passed is:

$$\Delta t = \frac{L_s}{U_s} \tag{31}$$

and the velocity of T with respect to T_1:

$$|\bar{V}_{T_1T}| = \frac{L_{T_1}}{\Delta t} = \frac{L_{T_1}}{L_s} U_s = L U_s \tag{32}$$

where L_{T_1} is the distance between T and T_1 and L is defined as L_{T_1}/L_s.

Law and Glass[15] have developed an analytical method by which the location of T_1 can be predicted in fairly good agreement with experiments. In their analysis they assumed the Mach stem to be straight and perpendicular to the wedge surface. Consequently, they arrived at the following empirical relation[15]

$$L_D = L_s[1 - (\rho_0/\rho_1)] \tag{33}$$

where L_D and L_s are defined in Fig. 5a. This result was later found by Bazhenova, et al.,[19] to be very good in the range $\theta_W < 40$ deg and fairly good elsewhere. Applying this result we

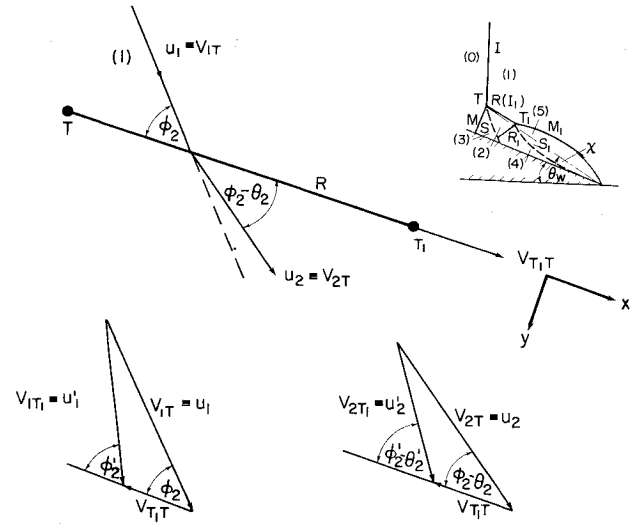

Fig. 6 Schematic diagram illustrating change in dynamic properties as measured from second triple point T_1, due to its motion with respect to first triple point T.

calculate:

$$L = (\rho_0/\rho_1) \operatorname{cosec} (\phi_1 + \phi_2 - \theta_1) \tag{34}$$

Inserting Eq. (34) into Eq. (32) yields:

$$|\bar{V}_{T_1T}| = (\rho_0/\rho_1) U_s \operatorname{cosec} (\phi_1 + \phi_2 - \theta_1) \tag{35}$$

Consider now Fig. 6 in which T_1 moves along the x axis (defined along the reflected shock wave R) at velocity $\bar{V}_{T_1T}$ with respect to T. Simple vector analysis yields that:

$$V^x_{1T_1} = V_{1T} \cos\phi_2 - V_{T_1T}$$

$$V^y_{1T_1} = V_{1T} \sin\phi_2$$

where V_{1T} is the flow velocity in region 1 with respect to T (i.e., $V_{1T} = U_1$) and $V^x_{1T_1}$ and $V^y_{1T_1}$ are the x and y components of the velocity of the flow in state 1 with respect to T_1, i.e., the x and y components of U_1'. The value of U_1' then becomes:

$$\begin{aligned} U_1' &= [(V^x_{1T_1})^2 + (V^y_{1T_1})^2]^{1/2} \\ &= (U_1^2 + V^2_{T_1T} - 2U_1 V_{T_1T} \cos\phi_2)^{1/2} \end{aligned} \tag{36}$$

whereas the value of ϕ_2' is:

$$\phi_2' = \tan^{-1} \frac{V^y_{1T_1}}{V^x_{1T_1}} = \tan^{-1} \left(\frac{U_1 \sin\phi_2}{U_1 \cos\phi_2 - V_{T_1T}} \right) \tag{37}$$

Inserting the value of V_{T_1T} from Eq. (35) into Eqs. (36) and (37) finally results in

$$U_1' = U_1 \left[1 + \frac{\sin^2(\phi_1 - \theta_1)}{\sin^2(\phi_2 + \phi_1 - \theta_1)} - 2 \frac{\sin(\phi_1 - \theta_1) \cos\phi_2}{\sin(\phi_2 + \phi_1 - \theta_1)} \right]^{1/2} \tag{38}$$

$$\phi_2' = \tan^{-1} \left[\frac{\sin\phi_2}{\cos\phi_2 - \sin(\phi_1 - \theta_1) \operatorname{cosec}(\phi_2 + \phi_1 - \theta_1)} \right] \tag{39}$$

Using trigonometric functions Eq. (39) can be simplified to:

$$\phi_2' = \phi_2 + \phi_1 - \theta_1 \tag{40}$$

Since all the variables in Eqs. (38) and (40) are known once Eqs. (2-15) are solved, one can calculate U_1' and ϕ_2'. Con-

sequently, the four parameters required for solving Eqs. (16-29) are analytically determined, and Eqs. (16-19) can be solved by the method presented earlier for the solution of Eqs. (2-15).

Prediction of Second Triple-Point Trajectory

It is clear from Fig. 5a that

$$\chi' = 90\,\text{deg} - \theta_w - \phi_1' \tag{41}$$

The velocity of T_1 with respect to the laboratory frame of reference can be written as

$$\bar{V}_{T_1L} = \bar{V}_{T_1T} + \bar{V}_{TL}$$

where $\bar{V}_{T_1T}$ is the velocity of T_1 with respect to T and $\bar{V}_{TL}$ is the velocity of T with respect to the laboratory frame of reference. Using the x, y coordinates of Fig. 5a, the x and y components of $\bar{V}_{T_1L}$ can be expressed as follows:

$$V^x_{T_1L} = \bar{V}_{TL}\sin\phi_1 - V_{T_1T}\sin\omega \tag{42}$$

$$V^y_{T_1L} = \bar{V}_{TL}\cos\phi_1 + V_{T_1T}\cos\omega \tag{43}$$

where ω is the angle between the incident and reflected shock waves (I and R).

If the frame of reference is attached to T_1 the angle of incidence ϕ_1' between the flow in state 0 and the incident shock wave is:

$$\phi_1' = \tan^{-1}(V^x_{T_1L}/V^y_{T_1L})$$

Inserting Eqs. (42) and (43) into the above expression and making use of Eqs. (30) and (32) results in

$$\phi_1' = \tan^{-1}\left[\frac{1 - L\sin\omega}{\cot\phi_1 + L\cos\omega}\right] \tag{44}$$

The angle ω can be expressed using Fig. 5b as follows

$$\omega = 180\,\text{deg} - (\phi_2 + \phi_1 - \theta_1) \tag{45}$$

Inserting Eqs. (34) and (45) into Eq. (44) yields

$$\phi_1' = \tan^{-1}\left[\frac{1 - \rho_0/\rho_1}{\cot\phi_1 - (\rho_0/\rho_1)\cot(\phi_2 + \phi_1 - \theta_1)}\right] \tag{46}$$

Upon inserting Eq. (46) into Eq. (41) one finally obtains

$$\chi' = 90\,\text{deg} - \theta_w - \tan^{-1}\left[\frac{1 - \rho_0/\rho_1}{\cot\phi_1 - (\rho_0/\rho_1)\cot(\phi_2 + \phi_1 - \theta_1)}\right] \tag{47}$$

Thus for a set of given initial conditions P_0, T_0, M_s, and θ_w, the value of χ (the first triple-point trajectory angle) can be calculated using the appropriate method.[1-3] Once χ is known, $\phi_1 = 90\,\text{deg} - \theta_w - \chi$ and $M_0 = M_s\,\text{cosec}\,\phi_1$ are obtained and Eqs. (2-15) can be solved since all the LHS parameters of Eqs. (2-5) are defined. The solution of Eqs. (2-15) provides the parameters required to calculate U_1' and ϕ_1' from Eqs. (38) and (40), respectively, that are needed for solving Eqs. (16-29) and to calculate χ' from Eq. (47).

The dependence of the second triple-point trajectory angle χ' upon the actual wedge angle θ_w for constant M_s for perfect and imperfect gases ($P_0 = 15$ Torr, $T_0 = 300$ K) is shown in Figs. 7a and 7b, respectively. It is seen that χ' decreases as θ_w and M_s increase. The curves corresponding to $M_s = 3$ and 10 are reproduced in Fig. 7c in order to examine the dependence of χ' upon the real gas effect. Figure 7c indicates that real gas effects increase the value of χ'. The stronger they are (i.e., the

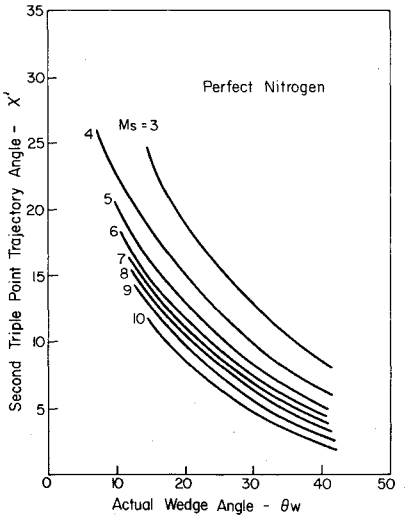

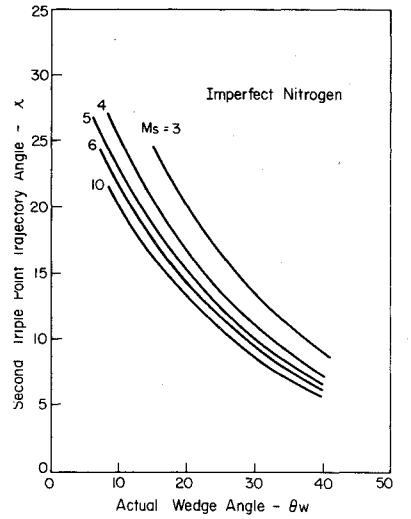

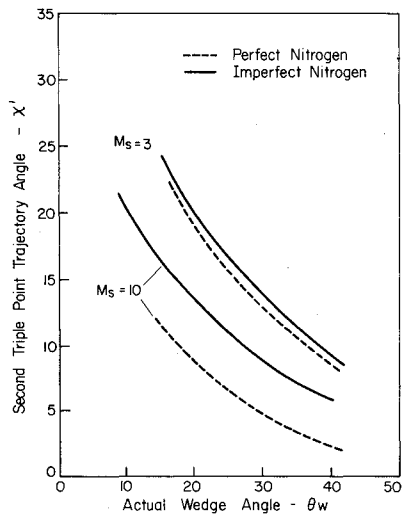

Fig. 7 Variation of second triple point χ' with wedge angle θ_w for a given incident shock-wave Mach number M_s: a) perfect diatomic gas $\gamma = 7/5$; b) imperfect nitrogen $P_0 = 15$ Torr, $T_0 = 300$ K; c) comparison between perfect and imperfect nitrogen for weak ($M_s = 3$) and strong ($M_s = 10$) incident shock waves.

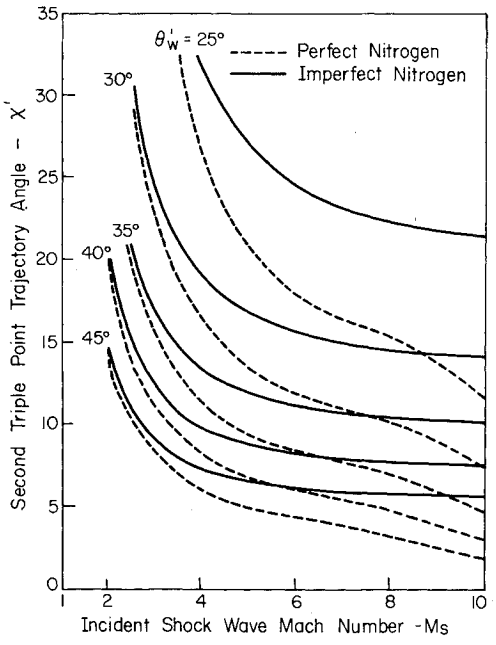

Fig. 8 Variation of χ' with M_s for a given θ'_w ($\theta'_w = \theta_w + \chi$): solid lines show imperfect nitrogen, $P_0 = 15$ Torr, $T_0 = 300$ K; dashed lines show perfect diatomic gas $\gamma = 7/5$.

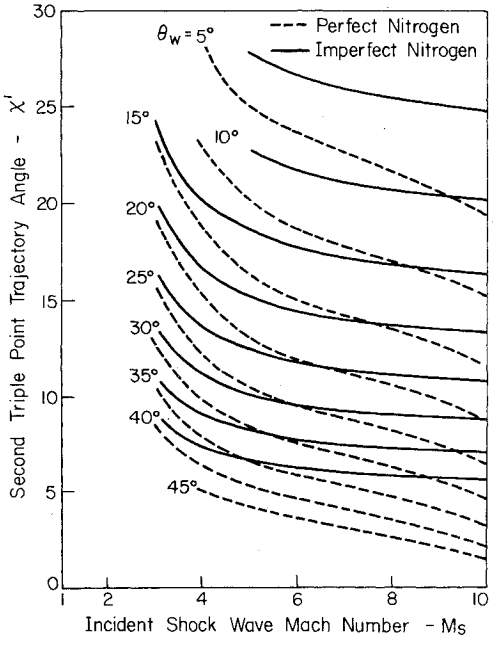

Fig. 9 Variation of χ' with M_s for given θ_w: solid lines show imperfect nitrogen $P_0 = 15$ Torr, $T_0 = 300$ K; dashed lines show perfect diatomic gas.

stronger M_s) the more they contribute to the value of χ'. The value of χ' as a function of the effective wedge angle θ'_w ($\theta_w + \chi$ or $\theta'_w = 90$ deg $- \phi_1$) and the incident shock-wave Mach number M_s for both perfect and imperfect nitrogen is shown in Fig. 8. Again it is seen that the imperfect gas value of χ' is greater than the perfect gas value. The larger M_s the larger the difference between these two values is. It is important to note that as M_s increases the imperfect gas lines (solid) level out, resulting in a situation in which χ' is independent of M_s, i.e., $\chi' = \chi'(\theta'_w)$ only. This is not the case for a perfect gas, where χ' continues to decrease as M_s increases. The value of χ' as a function of M_s with the actual wedge angle θ_w as a parameter is shown in Fig. 9. The dashed lines are again for perfect nitrogen and the solid line for imperfect nitrogen at $P_0 = 15$ Torr and $T_0 = 300$ K. Figure 9 indicates that for imperfect gases, χ' becomes independent of M_s at a high Mach number, resulting in a situation where $\chi' = \chi'(\theta_w)$ only. It is worth mentioning again that Figs. 7-9 were obtained analytically by solving Eqs. (2-15) and (47). Since Eqs. (2-15) also describe a SMR, values of χ' can also be obtained mathematically for cases where DMR does not exist by simply inserting the required values into Eq. (47). To the best of our understanding, these values have no physical meaning. However, it was decided to plot the resultant values of χ' for this case as well.

Graphical Solution of DMR

Like the analytical solution of DMR, the graphical solution is also done in two steps: first, the frame is reference is attached to the first triple point T and then it is attached to the second triple point T_1. First the I and R polars (Fig. 10a) are drawn in the same way they are drawn for SMR.[3,15] States 2 and 3 of Fig. 3 are at the point where I and R polars intersect. Note that all flow directions are measured with respect to the first triple-point trajectory, i.e., $\theta_0 = 0$ since the flow in state 0 moves parallel to the first triple-point trajectory and $\theta_2 = \theta_3$ since the flows in both sides of the slipstream are parallel. Consider Fig. 10b in which θ and θ' are two angles corresponding to an arbitrary direction measured from two different frames of reference at T and T_1, respectively.

Geometrical consideration yields

$$\theta = \theta' + (\chi' - \chi) \tag{48}$$

or alternatively

$$\theta = \theta' + (\phi_1 - \phi'_1) \tag{49}$$

where $\phi_1 = 90$ deg $- (\theta_w + \chi)$ and $\phi'_1 = 90$ deg $- (\theta_w + \chi')$ and ϕ'_1 is given by Eq. (46). Consequently, state 1 in a frame of reference attached to T_1 is at $\theta'_1 = \theta_1 - (\phi_1 - \phi'_1)$ and $P'_1 = P_1$ (no change in thermodynamic properties while changing the frame of reference). The flow Mach number in state 1 with respect to T_1 is obtained from Eq. (38) by dividing both the LHS and the RHS by the speed of sound a_1. States 2 and 3 are in a frame of reference attached to T_1, i.e., states 2′ and 3′ are at the point where a constant pressure line drawn from states 2 and 3 intersects the R' polar that corresponds to M'_1 and is drawn from state 1′. Once state 2′ is known the R_1 polar corresponding to M'_2, $P'_2 = P_2$, and $T'_2 = T_2$ is drawn. States 4′ and 5′ are at the point where the R_1 polar intersects the R' polar.

It should be mentioned that Henderson and Lozzi[16] presented a graphical solution of DMR. Unfortunately, however, their solution fails to account for the fact that the flows in states 1 and 2 move more slowly with respect to T_1 than they do with respect to T, owing to the relative motion between T and T_1. Their solution would be correct if the reflection process was steady and not pseudosteady as it is. Consequently, to the best of our knowledge, this is the first time that a graphical solution for DMR is presented.

Comparison with Experiments

The experimental data of a detailed study of the shock-wave reflection phenomenon[24] were used to check the accuracy of the present method for predicting χ'. The experiments were performed using the 10×18 cm UTIAS Hypervelocity Shock Tube. The process was recorded using a 23 cm-diam field of view Mach-Zehnder interferometer equipped with a giant-pulse, dual-frequency ruby laser.

Figure 11 is a reproduction of Fig. 9 for $\theta_w = 30$ and 40 deg that lie in the DMR domain (Fig. 2). While a very good agreement is obtained for $\theta_w = 30$ deg over the entire range of M_s, for $\theta_w = 40$ deg the agreement is good only for $M_s \leq 7$. In the range $M_s > 7$ the experimental values of χ' are smaller than the analytically predicted value. This we believe is probably due to the fact that in Eq. (47) (by which χ' is

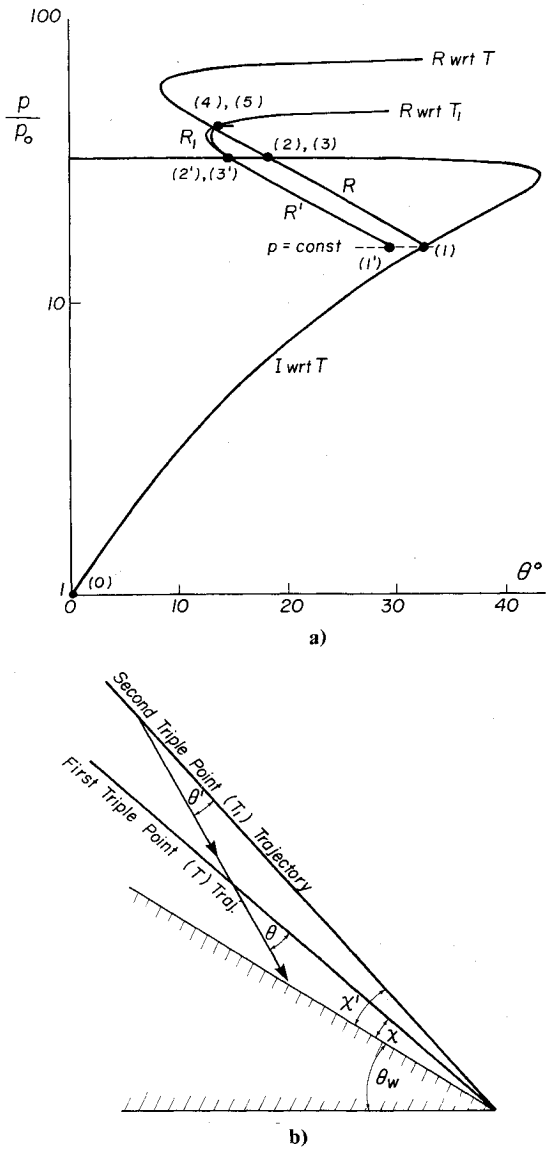

Fig. 10 Graphical solution of DMR: a) shock-polar presentation of DMR in pressure-deflection (P,θ) plane, nitrogen, $M_s = 4.68$, $\theta_w = 40$ deg, $\chi = 4.8$ deg, $P_0 = 15$ Torr, $T_0 = 297.4$; b) schematic diagram showing rotation involved in moving frame of reference from T to T_1.

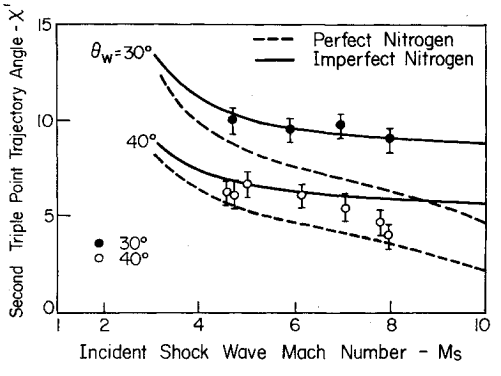

Fig. 11 Verification of χ' as function of M_s and θ_w: solid lines show imperfect nitrogen $P_0 = 15$ Torr, $T_0 = 300$ K; dashed lines show perfect diatomic gas $\gamma = 7/5$ (all data points are from present study).

predicted) we made use of Eq. (34) which is based upon the empirical Eq. (33) found by Bazhenova[19] to be very good in the range $\theta_w < 40$ deg and only fairly good elsewhere. It should be mentioned, however, that all of the experimental results lie between the perfect and the imperfect values. This might suggest that the flow is neither perfect nor in thermodynamic equilibrium, but in an intermediate nonequilibrium state.

Conclusions

During the present investigation the following have been achieved:

1) The equations describing the DMR were given and their solution (analytical) was presented.

2) The relative motion of the second triple point with respect to the first triple point was investigated and formulated empirically.

3) The graphical solution (shock-polar presentation) of a DMR was given.

4) An analytical method for the prediction of the second triple-point trajectory angle was developed. The results were compared with actual experiments and good agreement was obtained.

Consequently, it can be summarized that our reconsideration of DMR complements the existing work on RR and SMR. It has brought understanding to this important problem which is the building block of much more complicated processes involving blast and detonation waves.

It is worthwhile mentioning that two assumptions (both initiated by Law and Glass[15]) were used in developing the analyses for the predictions of the first and second triple-point trajectory angles. The Mach stem was assumed to be straight and normal to the wedge surface, and the location of the second triple point was assumed to follow Eq. (33). Unfortunately, these two assumptions are not accurate enough over the entire range of θ_w. While the first assumption is better for large wedge angles,[3,15] the second is very good only in the range $\theta_w < 40$ deg.[19] Consequently, better method for the prediction of χ and χ' are still required.

Acknowledgment

The experimental work reported in this paper was performed at the University of Toronto Institute for Aerospace Studies. I wish to thank I. I. Glass of UTIAS for his invaluable help during the course of this project. His advice and suggestions are gratefully acknowledged. The financial assistance from the National Research Council of Canada and the U.S. Air Force under Contract AF-AFOSR 77-3303 is gratefully acknowledged. I also wish to thank M. Kline for her assistance.

References

[1] Ben-Dor, G. and Glass, I. I., "Domains and Boundaries of Nonstationary Oblique Shock-Wave Reflections: I. Diatomic Gas," *Journal of Fluid Mechanics*, Vol. 92, Pt. 3, June 1979, pp. 459-496.

[2] Ben-Dor, G. and Glass, I. I., "Domains and Boundaries of Nonstationary Oblique Shock-Wave Reflections: II. Monatomic Gas," *Journal of Fluid Mechanics*, Vol. 96, Pt. 4, Feb. 1980, pp. 735-756.

[3] Ben-Dor, G., "Regions and Transitions of Nonstationary Oblique Shock-Wave Diffractions in Perfect and Imperfect Gases," University of Toronto Institute of Aeronautical Studies, Rept. 232, Aug. 1978.

[4] von Neumann, J., *Collected Works*, Vol. 6, Pergamon Press, New York, 1963.

[5] Smith, L. G., "Photographic Investigation of the Reflection of Plane Shocks in Air," OSRD Rept. 6271 or NORC Rept. A-350, 1945.

[6] Bleakney, W. and Taub, A. H., "Interaction of Shock-Waves," *Review of Modern Physics* Vol. 21, Oct. 1949, pp. 584-605.

[7] Fletcher, C. H., "The Mach Reflection of Weak Shock-Waves," Dept. of Physics, Princeton University, Technical Rept. II-4, June 1950.

[8] Jones, D. M., Martin, P. M., and Thornhill, C. K., "A Note on the Pseudo-Stationary Flow Behind a Strong Shock Diffracted or Reflected at a Corner," *Proceedings of Royal Society*, Series A, Vol. 205, 1951, pp. 238-248.

[9] White, D. R., "An Experimental Survey of the Mach Reflection of Shock-Waves," Dept. of Physics, Princeton University, Techical Rept. II-10, Aug. 1951.

[10] Jahn, R. G., "The Refraction of Shock-Waves at Gaseous Interface, I—Regular Reflection of Weak Shocks, II—Regular Reflection of Strong Shocks, III—Irregular Reflection," Dept. of Physics, Princeton University, Tech. Repts. II-16, II-18, II-19, 1954, 1955, 1956.

[11] Henderson, L. F., "On the Confluence of Three Shock-Waves in a Perfect Gas," *Aeronautical Quarterly*, Vol. XV, May 1964, pp. 181-197.

[12] Gvozdeva, L. G. and Predvoditeleva, O. A., "Experimental Investigation of Mach Reflection of Shock-Waves with Velocities of 1000-3000 m/sec in Carbon Dioxide Gas, Nitrogen and Air," *Soviet Physics, Doklady*, Vol. 10, No. 8, 1966.

[13] Gvozdeva, L. G., Bazhenova, T. V., Predvoditeleva, O. A., and Fokeev, V. P., "Mach Reflection of Shock-Waves in Real Gases," *Astronautica Acta*, Vol. 14, May 1969, pp. 503-508.

[14] Gvozdeva, L. G., Bazhenova, T. V., Predvoditeleva, O. A., and Fokeev, V. P., "Pressure and Temperature at the Wedge Surface for Mach Reflection of Strong Shock-Waves," *Astronautica Acta*, Vol. 15, Nos. 5 and 6, 1970, pp. 503-509.

[15] Law, C. K. and Glass, I. I., "Diffraction of Strong Shock-Waves by Sharp Compressive Corner," *CASI Transactions*, Vol. 4, No. 2, Jan. 1971, pp. 2-12.

[16] Henderson, L. F. and Lozzi, A., "Experiments on Transition of Mach Reflection," *Journal of Fluid Mechanics*, Vol. 68, Pt. 1, March 1975, pp. 139-155.

[17] Schneyer, G. P., "Numerical Simulation of Regular and Mach Reflection," *Physics of Fluids*, Vol. 18, No. 9, 1975, pp. 1119-1124.

[18] Gvozdeva, L. G. and Fokeev, V. P., "Transition from Mach to Regular Reflection and Domains of Various Mach Reflections," translated from *Fizika Goreniya i Vzryva*, Vol. 13/Jan.-Feb. 1977, pp. 102-110.

[19] Bazhenova, T. V., Fokeev, V. P., and Gvozdeva, L. G., "Regions of Various Forms of Mach Reflection and Its Transition to Regular Reflection," *Acta Astronautica*, Vol. 3, Jan.-Feb. 1976, pp. 131-140.

[20] Kutler, P. and Shankar, V., "Diffraction of a Shock-Wave by a Compression Corner—Pt. I: Regular Reflection," *AIAA Journal*, Vol. 5, Feb. 1977, pp. 197-203.

[21] Shankar, V., Kutler, P., and Anderson, D., "Diffraction of Shock-Waves by a Compression Corner—Pt. II: Single Mach Reflection," *AIAA Journal*, Vol. 16, Jan. 1978, pp. 4-5.

[22] Hornung, H. G. and Kychakoff, G., "Transition from Regular to Mach Reflection of Shock-Waves in Relaxing Gases," *Proceedings of 11th International Shock-Tube Symposium*, edited by B. Ahlborn, A. Hertzberg, and D. Russel, University of Washington Press, Seattle, July 1977.

[23] Ben-Dor, G. and Glass, I. I., "Nonstationary Oblique Shock-Wave Reflections: Acutal Isopyonics and Numerical Experiments," *AIAA Journal*, Vol. 16, Nov. 1978, pp. 1146-1153.

[24] Ben-Dor, G., "Nonstationary Oblique Shock-Wave Diffractions in Nitrogen and Argon-Experimental Results," University of Toronto Institute of Aeronautical Studies, Rept. 237, Nov. 1978.

[25] Molder, S., "Particular Conditions for the Termination of Regular Reflection of Shock-Waves," *CASI Transactions*, Vol. 25, No. 1, 1979, pp. 44-49.

[26] Parks, E. K., "Supersonic Flow in a Shock Tube of Divergent Cross Section," University of Toronto Institute of Aeronautical Studies, Rept. 18, May 1952.